Journal of Zhejiang University-SCIENCE B (Biomedicine & Biotechnology) in press
www.jzus.zju.edu.cn; www.springer.com/journal/11585
E-mail: jzus_b@zju.edu.cn

Research Article

https://doi.org/10.1631/jzus.B2500069

Improving the thermal stability of *trans*-epoxysuccinate hydrolase

Wenna BAO[1], Jinfeng YAO[1], Haifeng PAN[2]✉, Ronglin ZHU[1], Xinying LI[1], Hongxiu LIAO[1]

[1]*School of Biological and Chemical Engineering, Zhejiang University of Science and Technology, Hangzhou 310023, China*
[2]*School of Life Sciences and Health, Huzhou College, Huzhou 313000, China*

Abstract: This study used molecular dynamics simulations, B-factor analysis and saturation mutagenesis screening to enhance the thermal stability of the *trans*-epoxysuccinate hydrolase (TESH) derived from *Pseudomonas koreensis*. Eleven mutants that influence this characteristic were selected, yielding 4 mutants with improved activity. Among them, mutant A142C and S178Q exhibited lower Michaelis constant (K_m) values, and their k_{cat} (Catalytic constant)/K_m ratios were 4.7 and 1.9 times higher than those of the wild type. The half-life at 50°C ($T_{1/2}^{50}$) values of the two mutants were increased by 107% and 59%, respectively, compared to the wild type. Molecular docking and molecular dynamics simulations indicated that the two mutants showed stronger substrate interaction, lower binding energy, and reduced root mean square deviation compared to the wild type, along with decreased electrostatic potential energy and increased hydrophobicity near their mutation sites. The study of protein thermal stability engineering and associated mechanisms provides a valuable reference and holds practical significance for the industrial production of *meso*-tartaric acid.

Key words: *Trans*-epoxysuccinate hydrolase; *Pseudomonas koreana*; Molecular dynamics simulation; Thermal stability modification

Unedited

1 Introduction

Epoxide hydrolases (EHs; EC 3.3.2.3), which are widely distributed in nature and present in organisms such as animals, plants and microorganisms, require no cofactors to function. They are known to catalyze the enantioselective and regioselective addition of water molecules to the ethylene oxide ring of epoxides, resulting in optically active o-diols (Steinreiber and Faber, 2001). EHs from microbial sources are increasingly recognized as highly versatile biocatalysts for the preparation of enantiomeric pure epoxides and orthodiols, which form an important group of enantiomeric pure compounds in the chemical and pharmaceutical industries.

Epoxysuccinate hydrolase (ESH), a member of the EHs family, can hydrolyze epoxysuccinic acid into tartaric acid (TA), serving as a key enzyme in the synthesis of TA (Archelas and Furstoss, 1998). Owing to the presence of two asymmetric carbon atoms, TA exists in three optical isomeric forms, including *L*(+)-TA, *D*(−)-TA, and *meso*-TA. The reported ESHs are primarily derived from bacteria (Sato and Yanai, 1976; Kamatani et al., 1977; Prescher and Schreyer, 1979; Rosenberg et al., 1999; Cheng et al., 2014), and their stereoselectivity varies across different sources. These three TA isomers are associated with the corresponding ESHs, which are designated as CESH[L] (*cis*-ESH for *L*(+)-TA production), CESH[D] (*cis*-ESH for *D*(−)-TA production), and TESH (*trans*-ESH for *meso*-TA production), respectively (Sun et al., 2019). *Meso*-TA is relatively rare, typically found as ferrous tartrate, and used as an anti-salt caking agent (Prescher and Schreyer, 1979). It also has applications in snow removal, baking powder preparation, and medicine (Bao et al., 2015).

Recently, we characterized TESH from *Pseudomonas koreensis* and explored its catalytic mechanism (Liao et al., 2024). However, when incubated at 45°C for 30 min, only 10% of the residual activity of TESH remained, indicating its poor thermal stability. The modification of enzyme thermal stability not only improves enzyme performance but also enables effective application under a wide range of industrial scenarios and

✉ Haifeng PAN, haifengpan518@163.com
Haifeng PAN, https://orcid.org/0000-0002-3585-372X

Received Feb. 9, 2025; Revision accepted May 12, 2025;
Crosschecked xxx. xx, 20xx; Published online xxx. xx, 20xx

© Zhejiang University Press 2025

environments, playing a key role in many efficient and sustainable industrial processes. Bioinformatics are crucial in enzyme modification (Zhang et al., 2019). The B-factor is an important parameter in determining protein thermal stability. It reflects the movement and flexibility of atoms, amino acid side chains, and loop regions within protein structures. In general, a higher B-factor indicates greater atomic mobility and flexibility in a region, which corresponds to a more unstable structure; conversely, a lower B-factor suggests greater rigidity and structural stability (Tang et al., 2019; Carugo, 2022). Molecular dynamics simulations allow for the atomic-level simulation of protein systems, tracking the movement of molecules over time to uncover their dynamic properties. By simulating protein behavior under different conditions, such as variations in temperature, pH or ligand binding, these simulations can provide insights into the factors influencing protein stability and help understand their effects on protein structure and function (Sinha et al., 2022; Weng et al., 2023).

In this study, molecular dynamics simulation was conducted to identify its unstable regions, and B-factor analysis helped pinpoint hotspots with poor thermal stability. Subsequently, saturation mutagenesis simulation was carried out to select and optimize stability-enhancing mutations. Eleven mutants were selected, mutated and characterized, resulting in two mutants with improved thermal stability and enzymatic activity. The findings provide an important reference for the thermal stability engineering of proteins and hold practical significance for the industrial production of *meso*-TA.

Unedited

2 Materials and methods

2.1 Strain and plasmid

The TESH gene of *P. koreensis* (GenBank registration number no. WP_151550555) was cloned in our laboratory and expressed in *Escherichia coli* BL21 (DE3)-pET15b (+)-TESH (Liao et al., 2024).

2.2 Homology modeling and molecular thermal stability simulation

The model of TESH was generated using the SWISS-MODEL (Waterhouse et al., 2018) (https://swissmodel.expasy.org), and B-factor analysis was conducted using HOTSOPT WIZARE v3.1 (Sumbalova et al., 2018) (https://loschmidt.chemi.muni.cz/hotspotwizard). Discovery Studio 2019 was utilized for mutant stability energy calculation and molecular dynamics simulations. The energy effect of each mutation on protein stability (mutation energy, $\Delta\Delta G_{mut}$) was calculated as the difference in folding free energy between the mutant structure and the wild type protein, as expressed in Eq. (1):

$$\Delta\Delta G_{mut} = \Delta\Delta G_{folding}(\text{mutant}) - \Delta\Delta G_{folding}(\text{wild type}) \quad (1)$$

The folding free energy is defined as the difference in free energy between the folded and unfolded states of a protein, as expressed in Eq. (2):

$$\Delta\Delta G_{folding} = \Delta G_{fld} - \Delta G_{mut} \quad (2)$$

where ΔG_{fld} and ΔG_{unf} represent the free energy of the folded and unfolded (denatured) states.

2.3 Construction of site-directed mutations

Taking the results of pre-screening as a basis, mutation primers were designed (Table S1). Site-directed mutagenesis was performed using PrimeSTAR® Max DNA polymerase (Takara) and mutant primers, which were synthesized by Youkang Biological Company (Hangzhou, China).

2.4 Purification and characterization of enzymes

Wild type and mutant TESHs were expressed in *E.coli* BL21 (DE3) cells and purified using His-Tag protein agarose purified resin (Sangon Biotech, Shanghai, China) according to the method for CESH[D] (Bao et al., 2014). After desalting the protein by ultrafiltration, it was added with 20% glycerol at −20°C for future use.

The effect of the thermal stability of TESH was investigated according to the method used for CESH[L] (Wang et al., 2013). The relative activity of the assay under standard reactions was set to 100%. The Michaelis constant (K_m), Maximum reaction rate (V_{max}) and Catalytic constant (k_{cat}) values of the enzyme were determined using the Michaelis-Menten plot when the concentration of *trans*-epoxysuccinic acid was increased from 20 to 320 mmol/L. After incubating TESH at 50°C for different periods, the temperature of the enzyme was adjusted to 37°C and the normalized conditions of pH 8.0 were set for 30 min to determine its stability.

2.5 Enzyme activity detection

The amount of *meso*-TA was determined by HPLC on a chiral column (Chirex 3126 (D)-penicillanmin, 50 × 4.6 mm) at 60°C. The sample volume was 10 μL. The mobile phase consisted of 88% (volume fraction) 1 mmol/L copper acetate and 50 mnol/L ammonium acetate (pH 4.5) with 12% (volume fraction) isopropanol at a flow rate of 1 mL/min. Detection was performed at 280 nm (Cheng et al., 2014). TESH activity of one unit was defined as the amount of enzyme producing 1 μmol *meso*-TA per min at 37°C, pH 8.0. Specific activity was defined as the number of units per milligram of protein. Protein concentration was determined by the Bradford Protein Assay Kit (Shanghai, China).

2.6 Molecular docking and molecular dynamics simulation

Molecular docking and molecular dynamics simulations were performed using the Discovery Studio 2019 client with CHARMM36 force field. The system was solvated in explicit water and subjected to a two-step energy minimization procedure. The first step was to perform energy minimization for 1000 steps, and the second step was to conduct energy minimization for 2000 steps. This was followed by a heating phase where the temperature was gradually increased from 50 K to 323.15 K, which was then maintained throughout both the equilibration and production stages. Production molecular dynamics simulations of 100 ns duration were conducted for both wild type and mutant proteins with whole sequence at 323.15 K temperature and 1 bar. Structural stability and flexibility were assessed by calculating root mean square deviation (RMSD) and root mean square fluctuation (RMSF) using the initial conformation as the reference (Da Fonseca et al., 2024; Liao, et al., 2024). For molecular docking, based on the previous research on the important active sites and catalytic mechanisms, the catalytic triad of Asp104-His272-Asp128 had been obtained (Liao et al., 2024). The region of this active center was selected for molecular docking, and the pose cluster radius was set to 0.1 nm.

3 Results and discussion

3.1 Homology modeling and dynamic simulation of TESH

The model used for molecular dynamics simulations was based on the 4nvr template (Liao et al., 2024), with homologous modeling conducted using the SWISS-MODEL. The sequence similarity between the template and TESH was 52.43%. In the model assessment of SWISS-MODEL, the Global Model Quality Estimation (GMQE) value stood at 0.70, and the GMEAN value was 0.76±0.05 (Fig. S1). On the other hand, the conformational validity of the TESH homology model was evaluated using a Ramachandran plot (Fig. S2). This plot categorizes amino acid residues into four regions: most favored region (90.7%), allowed region (8.8%), generously allowed region (0.5%), and disallowed region (0.4%). For the assessment of homology models, it is generally accepted that the proportion of amino acids located in the disallowed region should be less than 5% of the total residues. Given this criterion, the constructed model exhibited high reliability and was deemed suitable for subsequent applications.

Unedited

The simulation involved the pure protein under the CHARMM36 forcefield at 323.15 K (50℃) for 100 ns, during which the RMSD and RMSF values were calculated. The RMSD value serves as an indicator of protein stability, with lower RMSD values indicating reduced flexibility and greater stability. The simulations of wild type TESH (Fig. 1a) revealed that the RMSD initially increased during the first 25 ns and then fluctuated between 1.25 and 1.2 nm from 25 to 75 ns. However, after 75 ns, the RMSD began to rise steadily, suggesting that its insufficient stability at 50℃.

RMSF values, which assess the flexibility of amino acid residues, identified regions with high flexibility that correlate with structural instability. As shown in Fig. 1b, the RMSF values were elevated in three red-highlighted regions, underscoring the critical role of these residues in the thermal stability of the enzyme.

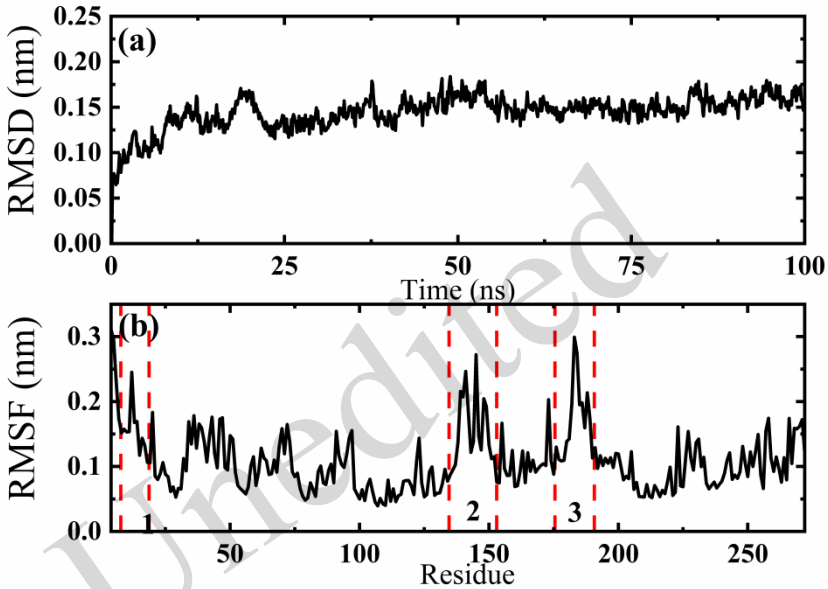

Unedited

Fig. 1 Molecular dynamics simulation of wild type TESH

(a) RMSD values for wild type TESH. (b) RMSF values for wild type TESH.

3.2 Thermal stability analysis

The B-factor rankings of amino acid positions were calculated using HOTSPOT WIZARD v3.1, and the top 20 positions were selected for further analysis (Table S2). The B-factor reflects the thermal motion or positional uncertainty of amino acid residues, with higher values indicating greater mobility or structural instability (Sun et al., 2019; Carugo, 2022). The results showed that the highest-ranking positions were predominantly located in the second and third highlighted regions identified in the molecular dynamics simulation. These regions included residues in the hydrogen bond corners, α-helices, and loop regions (Table 1).

The RMSF reflects the time-averaged flexibility of residues in the solution state (dynamic environment), which can identify functionally critical dynamic regions (such as catalytic sites, allosteric regulatory regions). The B-factor characterizes the spatial disorder of residues in the crystalline state, primarily influenced by lattice packing and static conformations. The integrated analysis of both methods not only provides multi-scale validation spanning from dynamic simulations to static structural data but also enables the balanced optimization of rigidity enhancement and functional preservation in thermostability engineering, thereby offering a critical foundation for the rational design of mutation strategies.

Although the optimal temperature of wild type enzyme was 50℃, its structural stability was significantly decreased. Therefore, residues in this region were subjected to saturation mutagenesis at 50℃. Stability assessments indicated that the mutation energy (ΔG_{mut}) below −0.5 kcal/mol were associated with a stable state. Based on these criteria, 11 mutants were selected for further investigation. Among them, R145I was considered

neutral, while the remaining 10 showed enhanced stability. Although mutations in Q138I, N140I and R145I led to reduced mutation energy, their stabilizing effects were less pronounced. In contrast, the other mutants exhibited significant improvements.

By combining B-factor analysis with molecular dynamics simulation results, the following 11 mutants were selected for further analysis: Q138I, T139W, N140I, A142C, A144F, R145I, S178Q, S180N, A181N, L183W, and K184L (Table 1). All of these residues were situated within the cap domain of the TESH structure (Fig. 2), which was consistent with the results by Taylor (1999), suggesting that the cap domain plays a crucial role in maintaining the overall structural stability.

B-factor analysis serves as a core tool for identifying thermolabile sites of an enzyme, and it is frequently integrated with other computational biology approaches to enhance the precision of a potential target. Han et al. (2019) identified the highly flexible region (residues 87-QNSS-90) in a fungal GH11 xylanase through B-factor analysis. By combining this with multiple sequence alignment, they observed that homologous thermophilic enzymes exhibited conserved residues 87-RGHT-90 at this site. Therefore, four single mutants (Q87R, N88G, S89H, S90T) were constructed, all of which showed significantly improved thermostability. Zhu et al. (2022) further expanded this strategy in engineering the thermostability of glutathione bifunctional synthase (GshFSA) from Streptococcus agalactiae. By coupling B-factor-screened high-fluctuation residues with unfolding free energy calculations, they obtained mutants R270S and Q406M with 2.62-fold and 3.02-fold increase in half-life period compared to the wild type, respectively. In this study, we integrated B-factor analysis with full-atom molecular dynamics simulations, employing dual criteria—static flexibility (B-factor) and dynamic fluctuations (RMSF), yielding the identification of 11 high-confidence thermolabile residues. This highlights the superior efficacy of integrating static and dynamic analyses in thermostability engineering.

Unedited

Table 1 Mutant B-factor ranking and mutational energy

Position	Secondary structure	B-factor rank	Mutant	Mutation Energy(kcal/mol)
Q138	hydrogen bonded turn	9	Q138I	-0.87
T139	Loop	7	T139W	-2.18
N140	Loop	4	N140I	-0.68
A142	Alpha helix	3	A142C	-1.06
A144	Alpha helix	8	A144F	-1.38
R145	Alpha helix	11	R145I	-0.3
S178	hydrogen bonded turn	6	S178Q	-1.28
S180	hydrogen bonded turn	2	S180N	-1.33
A181	hydrogen bonded turn	1	A181N	-1.22
L183	hydrogen bonded turn	5	L183W	-2.41
K184	hydrogen bonded turn	10	K184L	-2.40

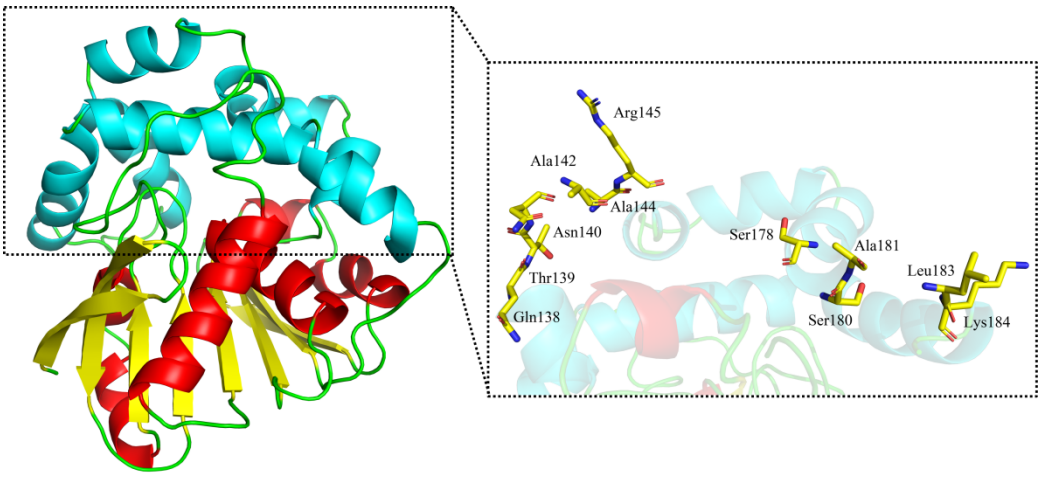

Fig. 1 Molecular dynamics simulation of wild type TESH

The cap domain is composed of α-helices (marked in blue), and the core domain consists of α-helices (marked in red) and β-sheets (marked in yellow). Other secondary structures were marked in green. The 11 thermal stability residues to be modified were shown.

3.3 Characterization of mutants

Site-directed mutagenesis by PCR was carried out, and their PCR products (Fig. S3) were transferred into *E. coli* BL21 (DE3) for expression. The wild type and mutant TESHs were purified using nickel affinity chromatography, with the results shown in Fig. 3. The bands of all mutants were relatively single, indicating high purity. The expression level of target protein varies across different mutants and the expression of mutant Q138I was the lowest. Kinetic analysis of each mutant (Table 2) showed that Q138I, T139W and A144F nearly lost enzyme activity. Conversely, mutants A142C, R145I, S178Q, and K184L displayed enhanced activity compared to the wild type, while the remaining mutants also decreased to varying degrees. Notably, A142C and S178Q exhibited lower K_m values than the wild type, indicating an improved affinity for the substrate. In contrast, most of the other mutants showed an increase in K_m values. The catalytic efficiency, represented by the k_{cat}/K_m ratio, was higher for A142C, S178Q, S180N, and K184L compared to the wild type, further underscoring their enhanced performance.

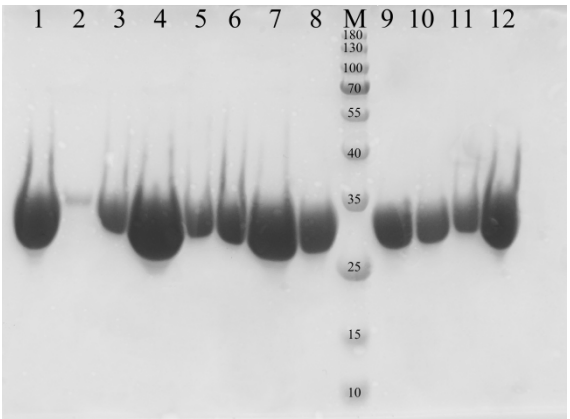

Fig. 3 SDS-PAGE analysis of purified TESHs

(1) wild type; (2) Q138I; (3) T139W; (4) N140I; (5) A142C; (6) A144F; (7) R145I; (8) S178Q; (9) S180N; (10) A181N; (11) L183W; (12) K184L; (M) Protein Marker

Unedited

Table 1 Mutant B-factor ranking and mutational energy

Enzyme	Relative activity (%)	K_m (mmol/L)	k_{cat} (s^{-1})	k_{cat}/K_m ($mmol/L^{-1}s^{-1}$)	$T_{1/2}^{50}$ (min)
Wild type	100±1.40	72.27	294.30	4.07	29.5
Q138I	4.03±0.19	n.a.	n.a.	n.a.	n.a.
T139W	4.73±1.20	n.a.	n.a.	n.a.	n.a.
N140I	29.80±1.27	507.6	501.94	0.99	6
A142C	130.77±1.43	25.40	486.74	19.16	61
A144F	1.73±0.05	n.a.	n.a.	n.a.	n.a.
R145I	179.07±1.85	130.2	76.52	0.59	3.5
S178Q	131.56±2.17	63.46	495.93	7.81	47
S180N	72.90±1.47	95.95	473.08	4.93	4.5
A181N	66.56±1.72	149.8	285.23	1.90	51
L183W	8.71±1.77	n.a.	n.a.	n.a.	n.a.
K184L	286.30±1.67	75.93	587.55	7.74	15

The enzyme activity of wild type TESH is 147.78 μmol/min/mg. n.a., not assayed due to low enzyme activity. Data are expressed as mean±standard deviation (SD), n=3.

3.4 Analysis of thermal stability

The specific activities of wild type and mutant TESHs after different incubation times were shown in Fig. 4. The enzyme activity of the wild type TESH gradually declined in the first 60 min, losing most of its activity during the period. Among the mutants, under the initial conditions of reaction at 37℃ for 30 min, the enzyme activity of A142C, R145I, S178Q, S180N, and K184L mutants was higher than that of wild type. After incubation at 50℃ for 15 min, the enzyme activity of R145I, S180N and K184L decreased significantly, falling below that of the wild type, indicating no improvement in thermal stability. In contrast, mutants A142C and S178Q exhibited higher initial enzyme activity than the wild type; their residual enzyme activity remained consistently higher with increasing time, showing a notable enhancement in thermal stability.

The residual enzyme activity of wild type and mutant TESHs at various times is shown in Fig. S4. The results indicate that the half-life at 50°C ($T_{1/2}^{50}$) values of A142C and S178Q increased by 107% and 59%, respectively, compared to the wild type. Among these two mutants, S178Q displayed better thermal stability during the first 45 min of incubation at 50℃. However, after 45 min, A142C showed superior thermal stability, retaining 40% of its enzyme activity after incubation for 90 min, while the wild type TESH showed a significant decline. Although the initial enzyme activity of A181N was lower than that of the wild type, its half-life at 50℃ $T_{1/2}^{50}$ increased by 73% after incubation for 90 min, with only a slight reduction in enzyme activity, indicating good thermal stability for this mutant.

Unedited

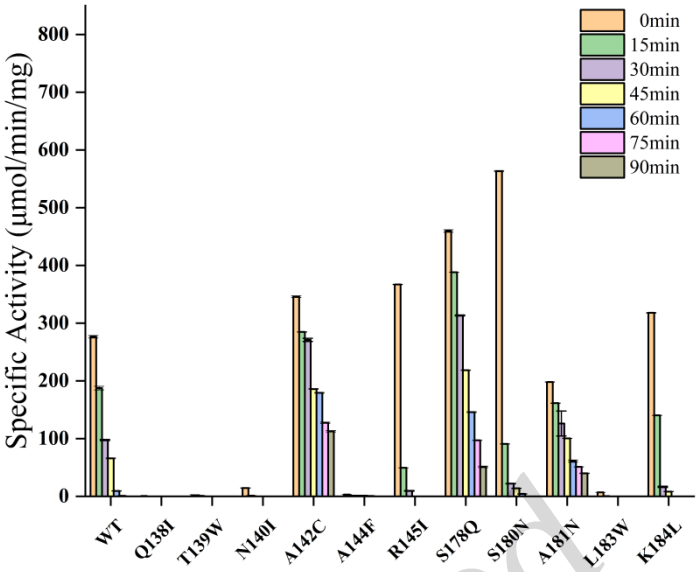

Fig. 4 Specific activity of wild type and mutant TESHs at different incubation times

Data are expressed as mean±standard deviation (SD), n=3.

Unedited

3.5 Molecular docking

Molecular docking of the wild type and mutant TESHs with the substrate (*trans*-epoxysuccinate) was performed. We selected the top-ranked conformation based on comprehensive scoring from the docking site heat map, which demonstrated higher confidence levels at multiple amino acid sites compared to other conformations (Fig. S5). The reliability of docking sites was further evaluated by calculating both the radius of gyration (R_g) and Jurs solvent accessible surface area (Jurs_SASA) values (Table S3). The R_g value reflects the relationship between conformational flexibility and spatial complementarity (Bhonsle et al., 2007), where lower values indicate more efficient conformational sampling and higher reliability. Jurs_SASA characterizes solvation effects and surface interactions, and a lower Jurs_SASA value suggests that the conformation may have formed a tighter binding interface (e.g., a hydrophobic pocket), resulting in reduced solvent exposure. Notably, both the R_g and Jurs_SASA values of the selected conformations were below average.

The docking energies were also calculated (Table S4). Except for certain mutants that largely lost enzyme activity and A181N, the binding energies of the remaining mutants decreased. Lower binding energy indicates a closer interaction between the enzyme and the substrate, leading to a more effective reaction, aligning well with the experimental results. For A181N, the binding energy showed minimal change compared to the wild type enzyme, consistent with its reduced activity observed in experiments. In the calculation of docking interaction energy, all six mutants exhibited decreased values. Notably, the mutants A142C and S178Q, which showed significant experimental improvements, also displayed substantial reductions in binding energy.

The docking results of the wild type and mutants A142C, S178Q, and A181N with substrate molecules are shown in Fig. 5. Compared to the wild type, the A142C mutant showed shorter bond lengths at several amino acid sites, indicating a closer interaction with the substrate. For example, the bond length at the Arg105 site was reduced from 0.52 nm to 0.417 nm, enhancing the attractive charge interaction to form a salt bridge. In addition, Arg108 formed a new conventional hydrogen bond with a bond length of 0.452 nm, which plays a key role in improving thermal stability (Hendsch and Tidor, 1994; Ban et al., 2021). Similarly, the S178Q mutant also showed varying degrees of bond length reduction in its interactions. At the Arg105 site, the bond length decreased from 0.52 nm to 0.414 nm, and this interaction was also enhanced to form a salt bridge. Arg108 formed an additional conventional hydrogen bond with a bond length of 0.45 nm. These docking results corroborate the

observed experimental improvements in the thermal stability of A142C and S178Q. In contrast, the docking results for A181N did not show significant differences from the wild type TESH. Notably, the Arg105 site did not participate in the reaction.

In summary, molecular docking indicated that the binding energy of the mutants A142C and S178Q decreased, the bond length of the interaction was shortened to varying degrees, and the binding to the substrate was closer. The Arg105 amino acid sites were all enhanced in the original attractive charge interaction force as a salt bridge, which played an important role in the thermal stability of the enzyme.

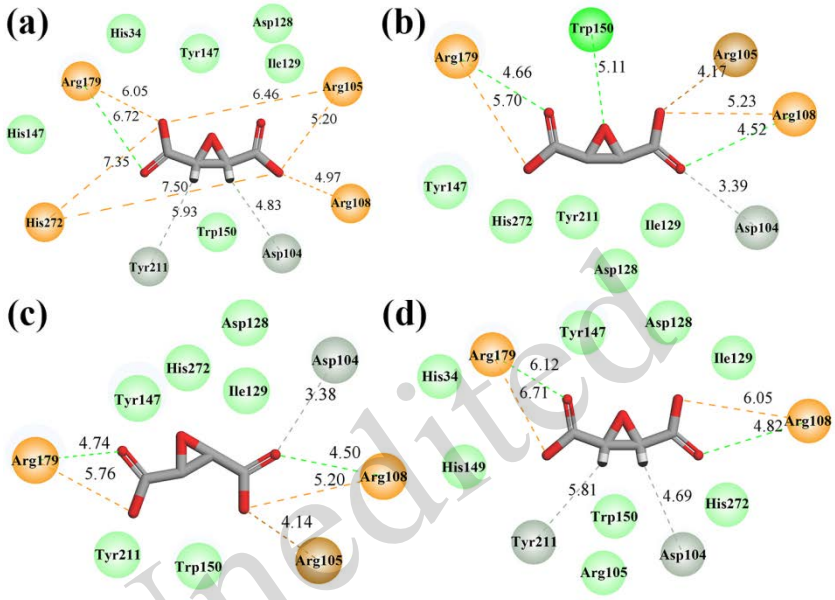

Fig. 5 Interaction of substrate binding sites

The amino acids near the binding pocket are shown and their interactions with substrate are represented by different colours. Light green represents van der Waals forces, dark green represents hydrogen bonds, dark brown represents salt bridges, light gray represents carbon hydrogen bonds, and orange represents charge interactions. (a). wild type; (b). A142C; (c). S178Q; (d). A181N.

Unedited

3.6 Molecular dynamics simulation of mutants

Molecular dynamics simulations were performed to calculate and compare the RMSD (Fig. 6) and RMSF (Fig. 7) values of the wild type and mutant variants, enabling a quantitative analysis of the effects of mutations on the structural stability and dynamic flexibility of TESH. The RMSD value is inversely correlated with protein stability: lower RMSD values indicate reduced flexibility, signifying a more stable protein structure, which is consistent with our experimental results. Among the three mutants that showed improved thermal stability in the experiments A142C, S178Q, and A181N, their RMSD values decreased to varying extents compared to the wild type, indicating enhanced stability (Fig. 6). These findings align with and confirm the experimental results.

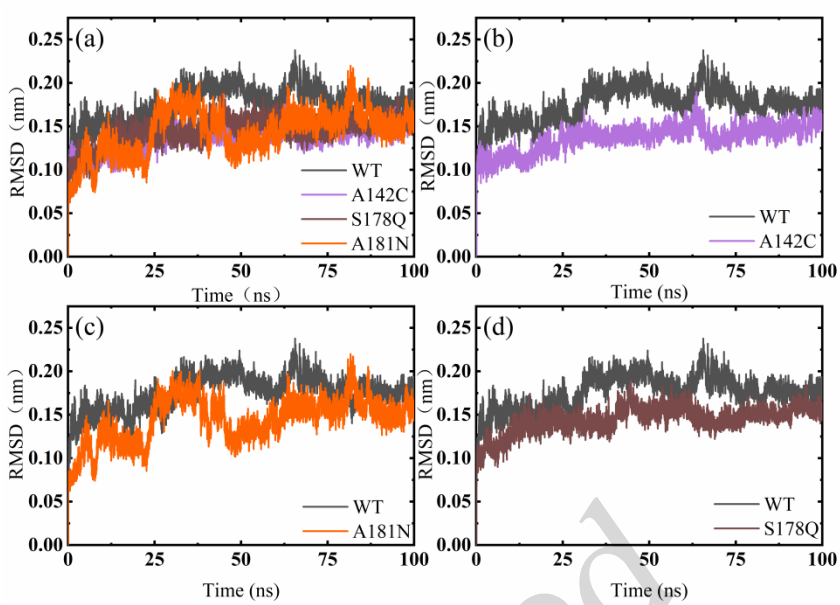

Fig. 6 RMSD values of wild type and mutant TESHs

(a) Comparison of RMSD values of wild type and 3 mutant TESHs. (b) Comparison of RMSD values of wild type and mutant A142C. (c) Comparison of RMSD values of wild type and mutant S178Q. (d) Comparison of RMSD values of wild type and mutant A181N.

Unedited

Next, comparative analyses of the RMSF values between wild type and three thermostable mutants (A142C, S178Q, and A181N) were carried out (Fig. 7). The mutant A142C exhibited reduced RMSF values around residue 142 compared to the wild type. Similarly, both S178Q and A181N showed decreased RMSF values near residue 180. These observed reductions in RMSF values suggested decreased conformational flexibility in these regions, making the structure more stable.

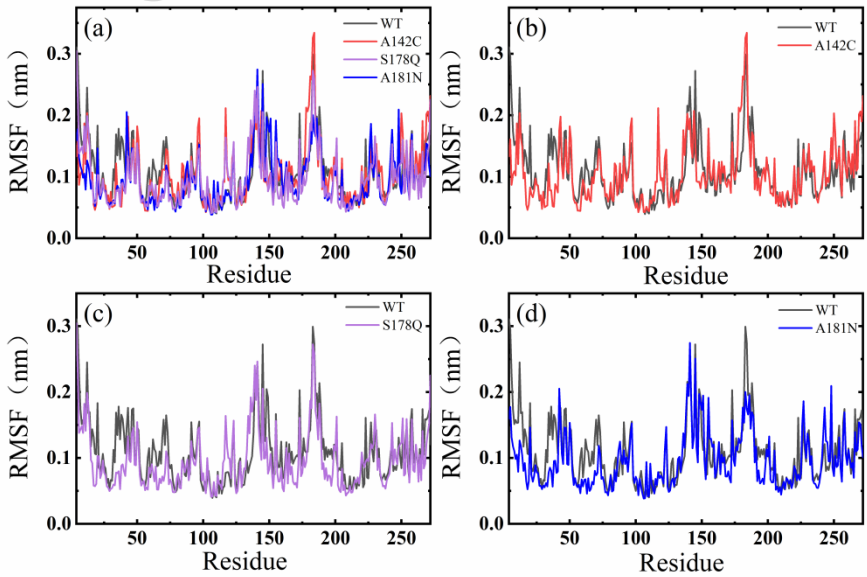

Fig. 7 RMSF values of wild type and mutant TESHs

(a) Comparison of RMSF values of wild type and 3 mutant TESHs. (b) Comparison of RMSF values of wild type and mutant A142C. (c) Comparison of RMSF values of wild type and mutant S178Q. (d) Comparison of RMSF values of wild type and mutant A181N.

The analysis of electrostatic potential energy in the three mutants (Fig. 8) revealed varying degrees of reduction, with A142C exhibiting the lowest values. As is well known, surface charged groups play a crucial role in the structure and function (such as stability) of proteins (Stigter, et al., 1991). Our results suggested that mutants with less positive charge in the mutated region possess enhanced thermal stability. Concurrently, hydrophobic interactions mediated by van der Waals forces contribute to structural stabilization by forming robust internal frameworks that resist environmental perturbations (e.g., temperature or pH fluctuations), thereby preserving the native conformation and biological activity of the enzyme. While the A142C mutation site itself showed minimal changes, its surrounding regions displayed enhanced hydrophobicity, whereas S178Q and A181N exhibited direct hydrophobicity increases at their mutation sites, likely contributing to the observed thermal stability improvement (Fig. 9).

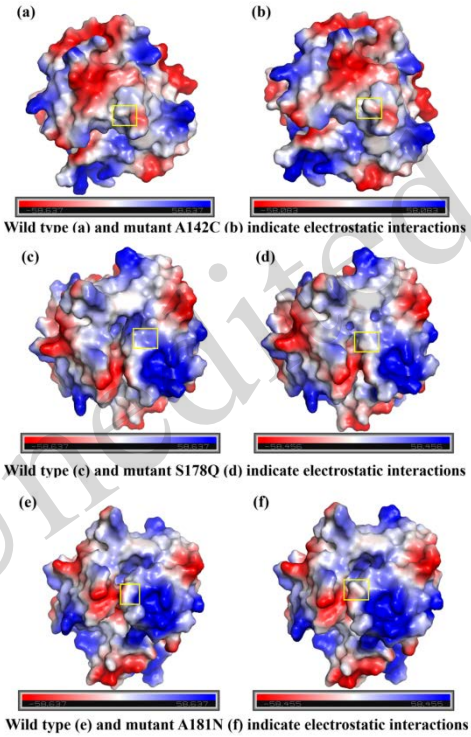

Unedited

Fig. 8 Surface electrostatic energy of wild type and mutants

The red regions represent negative charge, whereas the blue regions denote positive charge. The red-to-blue color gradient illustrates the continuous transition of charge from negative to positive properties.

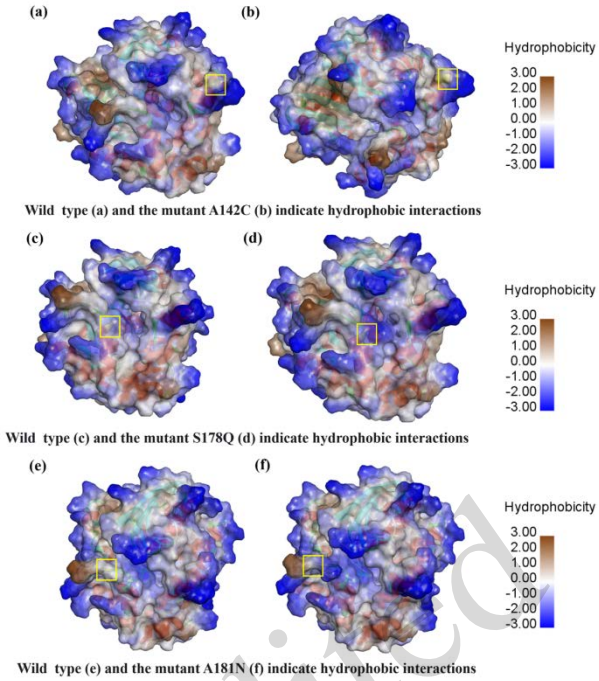

Fig. 9 Surface hydrophobic interactions of wild type and mutants

The blue regions represent hydrophobic areas, while the brown regions denote hydrophilic zones. The blue-to-brown color gradient illustrates the continuous transition from hydrophobic to hydrophilic characteristics.

The above findings demonstrate that single amino acid mutations could significantly alter enzymatic functional properties through multiple mechanisms. These structural mutations may modify the charge distribution and microenvironment of the active site, regulate the dynamic flexibility of protein conformation, or affect the spatial accessibility of substrate-binding channels, subsequently leading to functional alterations, such as changes in substrate selectivity (e.g., variations in Km values) and inhibitor sensitivity. This underscores the "single-site mutation → conformational adaptation → functional alteration" cascade mechanism in protein structures, establishing a theoretical framework for the comprehension and prediction of how mutations influence enzymatic function.

Unedited

4 Conclusions

In this work, bioinformatics methods were used to enhance the thermal stability of the TESHs from *P. koreensis*. Molecular dynamics simulations identified three unstable regions in the wild type TESH. Combining B-factor analysis and saturation mutagenesis screening, 11 sites that influence the thermal stability of the enzyme were selected, all of which were located in the cap domain. Four mutants with improved enzyme activity were obtained (A142C, R145I, S178Q, and K184L). Among them, mutant A142C and S178Q exhibited lower K_m values than the wild type, and their k_{cat}/K_m ratios were 4.7 and 1.9 times higher than those of the wild type, indicating that they got higher catalytic efficiency. The thermal stability experiment showed that the $T_{1/2}^{50}$ values of mutants A142C and S178Q were 2.1 and 1.6 times higher than that of the wild type, respectively. Furthermore, although the initial enzyme activity of the mutant A181N was lower than that of the wild type enzyme, its thermal stability was improved. Molecular docking analysis showed that the binding energies of mutants A142C and S178Q with the substrate were decreased, while new salt bridges were formed, which played a crucial role in the stability of the protein. Molecular dynamics simulations revealed that the RMSD and RMSF (around mutation sites) values of these two mutants were significantly lower than that of the wild type. The three thermostable mutants exhibited varying degrees of reduced electrostatic potential energy and increased

hydrophobicity in the vicinity of their mutation sites. The above findings provide a valuable reference for the thermal stability engineering of proteins, and holds practical significance for the industrial production of *meso*-TA.

Data availability statement

The dataset used or analyzed during the current study is available from the corresponding author on reasonable request.

Acknowledgments

This research was supported by the Zhejiang Province Scientific Research Project (No. Y202248484) and Huzhou Science and Technology Plan Project (2022GZ56) for their financial supports.

Author contributions

Wenna BAO: Conceptualization; supervision; experimental design; contributed to writing. Jinfeng YAO: Data curation; writing-original draft. Haifeng PAN: Data curation; review/edit manuscript; funding acquisition. Ronglin ZHU, Xinying LI and Hongxiu LIAO contributed to experimental research and data analysis. All authors have read and approved the final manuscript. Therefore, all authors have full access to all the data in the study and take responsibility for the integrity and security of data.

Compliance with ethics guidelines

Wenna BAO, Jinfeng YAO, Haifeng PAN, Ronglin ZHU, Xinying LI and Hongxiu LIAO declare that they have no conflicts of interest.

This article does not contain any studies with human or animal subjects performed by any of the authors

Unedited

References

Archelas A, Furstoss R, 1998. Epoxide hydrolases: New tools for the synthesis of fine organic chemicals. Trends in Biotechnology, 16(3):108-116.
https://doi.org/10.1016/S0167-7799(97)01161-X

Ban X, Xie X, Li C, et al., 2021. The desirable salt bridges in amylases: Distribution, configuration and location. Food Chemistry, 354:129475.
https://doi.org/10.1016/j.foodchem.2021.129475

Bao W, Pan H, Zhang Z, et al., 2014. Analysis of essential amino acid residues for catalytic activity of *cis*-epoxysuccinate hydrolase from *Bordetella* sp. BK-52. Applied Microbiology and Biotechnology, 98(4):1641-1649.
https://doi.org/10.1007/s00253-013-5019-2

Bao W, Pan H, Zhang Z, et al., 2015. Isolation of the stable strain *Labrys* sp. BK-8 for L(+)-tartaric acid production. Journal of Bioscience and Bioengineering, 119(5):538-542.
https://doi.org/10.1016/j.jbiosc.2014.10.013

Bhonsle, J.B., Venugopal, D., Huddler, D.P., et al., 2007. Application of 3D-QSAR for identification of descriptors defining bioactivity of antimicrobial peptides. Journal of Medicinal Chemistry, 50(26):6545-6553.
https://doi.org/10.1021/jm070884y

Carugo O, 2022. B-factor accuracy in protein crystal structures. Acta Crystallographica Section D, 78(1):69-74.
https://doi.org/doi:10.1107/S2059798321011736

Cheng Y, Wang L, Pan H, et al., 2014. Purification and characterization of a novel *cis*-epoxysuccinate hydrolase from *Klebsiella* sp. That produces L(+)-tartaric acid. Biotechnology Letters, 36(11):2325-2330.
https://doi.org/10.1007/s10529-014-1614-2

Da Fonseca AM, Caluaco BJ, Madureira JMC, et al., 2024. Screening of potential inhibitors targeting the main protease structure of SARS-CoV-2 via molecular docking, and approach with molecular dynamics, RMSD, RMSF, H-bond, SASA and MMGBSA. Molecular Biotechnology, 66(8):1919-1933.
https://doi.org/10.1007/s12033-023-00831-x

Han, N, Ma, Y, Mu, Y, et al., 2019. Enhancing thermal tolerance of a fungal GH11 xylanase guided by B-factor analysis and multiple sequence alignment. Enzyme and Microbial Technology, 131, p.109422.
https://doi.org/10.1016/j.enzmictec.2019.109422

Hendsch ZS, Tidor B, 1994. Do salt bridges stabilize proteins? A continuum electrostatic analysis. Protein Science, 3(2):211-226.
https://doi.org/10.1002/pro.5560030206

Kamatani Y, Okazaki H, Imai K, et al., 1977. Production of L(+)-tartaric acid. US Patent 4011135A.

Liao H, Pan H, Yao J, et al., 2024. Essential amino acid residues and catalytic mechanism of *trans*-epoxysuccinate hydrolase for

production of *meso*-tartaric acid. Biotechnology Letters, 46(5):739-749.
https://doi.org/10.1007/s10529-024-03490-3

Prescher G, Schreyer G, 1979. Process for the production of pure racemic acid and *meso*-tartaric acid and separation of maleic acid from synthetic tartaric acid. US Patent 4150241A.

Rosenberg M, Miková H, Krištofíková L, 1999. Production of L(+)-tartaric acid by immobilized bacterial cells *Nocardia tartaricans*. Biotechnology Letters, 21(6):491-495.
https://doi.org/10.1023/A:1005592104426

Sato E, Yanai A, 1976. Method for preparing d-tartaric acid. US Patent 3957579A.

Sinha S, Tam B, Wang SM, 2022. Applications of molecular dynamics simulation in protein study. Membranes, 12(9):844.
https://doi.org/10.3390/membranes12090844

Steinreiber A, Faber K, 2001. Microbial epoxide hydrolases for preparative biotransformations. Current Opinion in Biotechnology, 12(6):552-558.
https://doi.org/10.1016/S0958-1669(01)00262-2

Stigter, D., Alonso, D.O. Dill, K.A., 1991. Protein stability: electrostatics and compact denatured states. Proceedings of the National Academy of Sciences, 88(10):4176-4180.
https://doi.org/10.1073/pnas.88.10.4176

Sumbalova L, Stourac J, Martinek T, et al., 2018. Hotspot wizard 3.0: web server for automated design of mutations and smart libraries based on sequence input information. Nucleic Acids Research, 46(1):356-362.
https://doi.org/10.1093/nar/gky417

Sun Z, Liu Q, Qu G, et al., 2019. Utility of B-factors in protein science: Interpreting rigidity, flexibility, and internal motion and engineering thermostability. Chemical Reviews, 119(3):1626-1665.
https://doi.org/10.1021/acs.chemrev.8b00290

Tang H, Shi K, Shi C, et al., 2019. Enhancing subtilisin thermostability through a modified normalized B-factor analysis and loop-grafting strategy. Journal of Biological Chemistry, 294(48):18398-18407.
https://doi.org/10.1074/jbc.RA119.010658

Taylor WR, 1999. Protein structural domain identification. Protein Engineering, Design and Selection, 12(3):203-216.
https://doi.org/10.1093/protein/12.3.203

Wang Z, Wang Y, Su Z, 2013. Purification and characterization of a *cis*-epoxysuccinic acid hydrolase from *Nocardia tartaricans* CAS-52, and expression in *Escherichia coli*. Applied Microbiology and Biotechnology, 97(6):2433-2441.
https://doi.org/10.1007/s00253-012-4102-4

Waterhouse A, Bertoni M, Bienert S, et al., 2018. SWISS-MODEL: homology modelling of protein structures and complexes. Nucleic Acids Research, 46(1):296-303.
https://doi.org/10.1093/nar/gky427

Weng J, Yang S, Shen J, et al., 2023. Molecular dynamics simulation reveals DNA-specific recognition mechanism via c-Myb in pseudo-palindromic consensus of mim-1 promoter. Journal of Zhejiang University-SCIENCE B, 24(10):883-895.
https://doi.org/10.1631/jzus.B2200634

Zhang Y, Geary T, Simpson BK, 2019. Genetically modified food enzymes: a review. Current Opinion in Food Science, 25:14-18.
https://doi.org/10.1016/j.cofs.2019.01.002

Zhu W, Sun H, Jiang Q, et al., 2022. Enhancing the thermal stability of glutathione bifunctional synthase by B-factor strategy and un/folding free energy calculation. Catalysts. 15;12(12):1649.
https://doi.org/10.3390/catal12121649

Supplementary information:

Figs. S1-S5; Table S1-S4

Unedited

Supplementary materials

Table S1 Primers used herein

Primer name	Sequence(5'to3')
PrimerF1-Q138I	GCATGTATGCGATTACCAACGAAGC
PrimerR1-Q138I	GCTTCGTTGGTAATCGCATACATGC
PrimerF1-T139W	CATGTATGCGCAGTGGAACGAAGCGTTTG
PrimerR1-T139W	CAAACGCTTCGTTCCACTGCGCATACATG
PrimerF1-N140I	GTATGCGCAGACCATTGAAGCGTTTGCGC
PrimerR1-N140I	GCGCAAACGCTTCAATGGTCTGCGCATAC
PrimerF1-A142C	CAGTACGCGCGGGCAAAGCATTCGTTGGTTTGGGCGT
PrimerR1-A142C	ACGCCCAAACCAACGAATGCTTTGCCCGCGCGTACTG
PrimerF1-A144F	CAACGAAGCGTTTTTTCGCGCGTATTGG
PrimerR1-A144F	CCAATACGCGCGAAAAAACGCTTCGTTG
PrimerF1-R145I	CGAAGCGTTTGCGATTGCGTATTGGCATTG
PrimerR1-R145I	CAATGCCAATACGCAATCGCAAACGCTTCG
PrimerF1-S178Q	GAGCCCCGCACTACGCTGGCCCATCACACTGCG
PrimerR1-S178Q	CGCAGTGTGATGGGCCAGCGTAGTGCGGGGCTC
PrimerF1-S180N	GAGCCCCGCATTACGACTGCCCATCACACT
PrimerR1-S180N	AGTGTGATGGGCAGTCGTAATGCGGGGCTC
PrimerF1-A181N	GATGGGCAGCCGCAGCAATGGCCTGAAACCGTTTAC
PrimerR1-A181N	GTAAACGGTTTCAGGCCATTGCTGCGGCTGCCCATC
PrimerF1-L183W	TTCGTGAGTAAACGGTTTCCACCCCGCACTACGACTGCC
PrimerR1-L183W	GGCAGTCGTAGTGCGGGGTGGAAACCGTTTACTCACGAA
PrimerF1-K184L	CTTCGTGAGTAAACGGTAAGAGCCCCGCACTACGAC
PrimerR1-K184L	GTCGTAGTGCGGGGCTCTTACCGTTTACTCACGAAG

Table S2 B-factor analysis of important amino acid sites

Position	Residue	Secondary Structure	B-factor Rank
181	Ala	hydrogen bonded turn	1
180	Ser	hydrogen bonded turn	2
182	Gly	hydrogen bonded turn	3
141	Glu	alpha helix	4
179	Arg	bend	5
142	Ala	alpha helix	6
140	Asn	loop	7
183	Leu	hydrogen bonded turn	8
143	Phe	alpha helix	9
178	Ser	hydrogen bonded turn	10
139	Thr	loop	11
144	Ala	alpha helix	12
184	Lys	hydrogen bonded turn	13
177	Gly	hydrogen bonded turn	14
138	Gln	hydrogen bonded turn	15
145	Arg	alpha helix	16
185	Pro	hydrogen bonded turn	17
1	Met	loop	18
146	Ala	alpha helix	19
176	Met	alpha helix	20

Unedited

Table S3 Conformational Analysis of Molecular Docking

	Wild type		A142C		S178Q		A181N	
Conformation	R_g	Jurs_SASA	R_g	Jurs_SASA	R_g	Jurs_SASA	R_g	Jurs_SASA
1	2.05961	271.962	2.06554	272.694	2.05741	272.775	2.06024	271.551
2	2.06504	272.356	2.05517	272.302	2.07361	272.795	2.07217	276.173
3	2.06798	275.749	2.08098	273.526	2.06252	275.948	2.05613	276.979
4	2.0523	276.202	2.06275	275.647	2.05634	274.1	2.05923	275.908
5	2.06871	274.199	2.07528	276.738	2.06663	272.261	2.06051	275.449
6	2.05434	275.479	2.05702	277.555	2.05657	274.648	2.07487	277.09
7	2.07191	273.354	2.05308	276.05	2.048	276.961	2.06316	274.837
8	2.06227	276.406	2.06625	274.924	2.0374	274.577	2.07739	273.792
9	2.07629	273.466	2.05318	274.595	2.06632	274.964	2.05983	275.221
10	2.04494	274.682	2.04529	275.942	2.01954	270.557	2.06833	274.245
11	2.0647	273.711	2.05958	273.257	2.06866	275.035	2.03197	271.947
12	2.06849	274.29	2.05766	275.205	2.04844	276.411	2.04591	275.314
13	2.05605	272.819	2.0496	275.012	2.11279	279.371	2.03867	273.462
14	2.06016	276.562	2.03527	273.924			2.06769	276.633
15	2.0463	277.107	2.0564	275.409			2.06512	276.998

S178Q exhibited only 13 conformations.

Table S4 Energy calculation of molecular docking between wild type and mutants

Name	CDCOKER_ENERGY （kcal/mol）	CDOCKER_INTERACTION_ENERGY （kcal/mol）	Bingding_Energy （kcal/mol）
Wild type	-31.7662	-39.3276	-188.442
A142C	-33.4662	-41.4691	-205.853
R145I	-33.3692	-41.674	-207.802
S178Q	-33.6709	-41.7843	-209.174
S180N	-33.2882	-41.3444	-196.116
A181N	-31.6475	-39.3514	-190.208
K184L	-33.3057	-41.7174	-217.286

Unedited

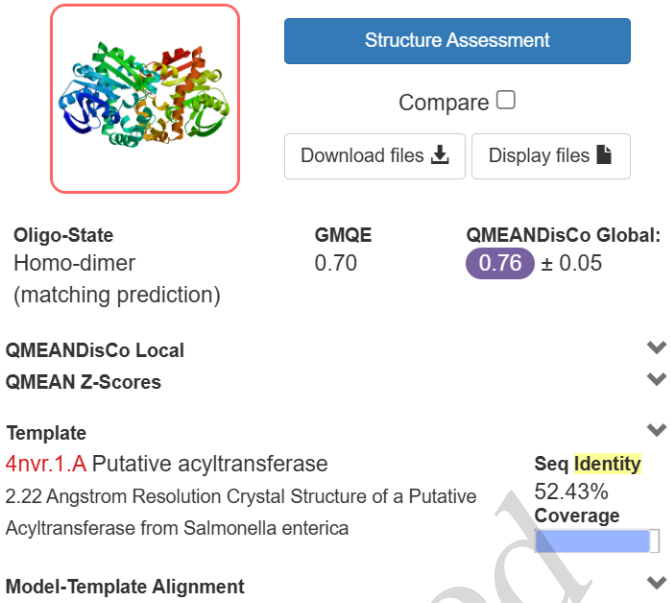

Fig. S1 Evaluation of the rationality of homology modelling

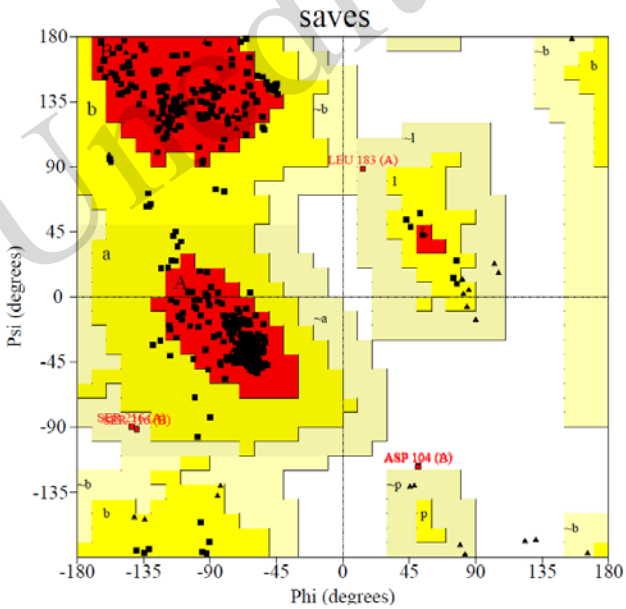

Fig. S2 Ramachandran plot of homology modelling

Unedited

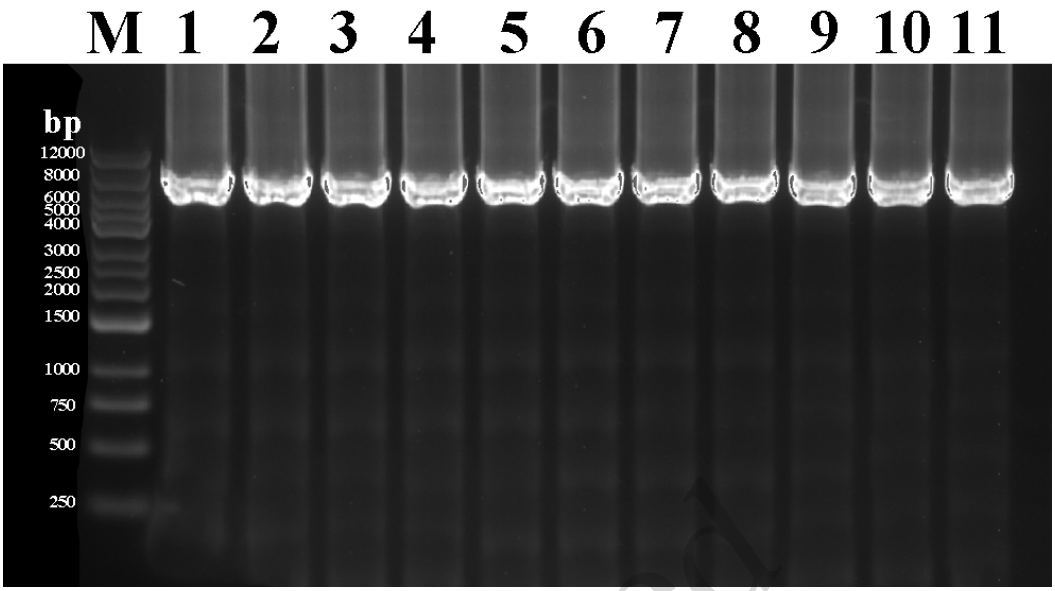

Fig. S3 Site-directed mutagenesis by PCR

(1) Q138I; (2) T139W; (3) N140I; (4) A142C; (5) A144F; (6) R145I; (7) S178Q; (8) S180N; (9) A181N; (10) L183W; (11) K184L

Unedited

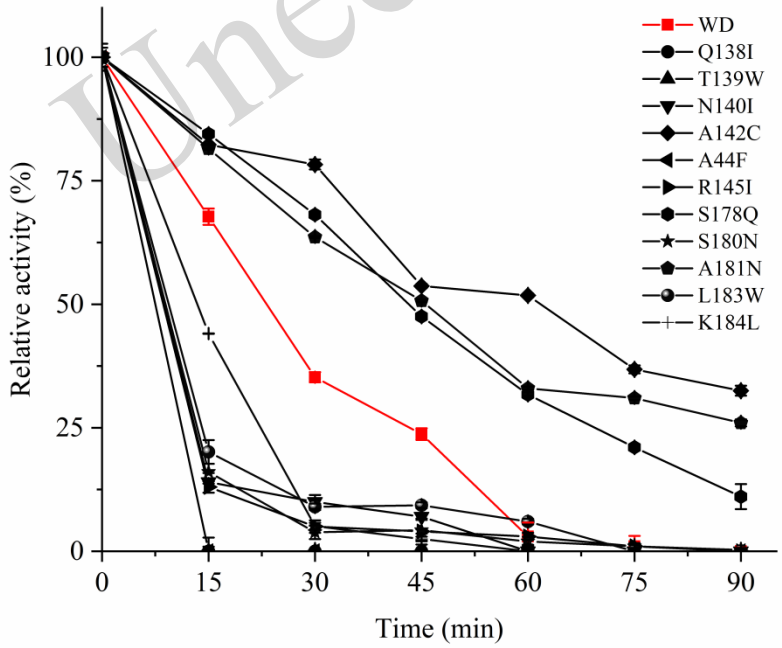

Fig. S4 Comparison of wild type and mutant inactivation curves

Data are expressed as mean±standard deviation (SD), n=3.

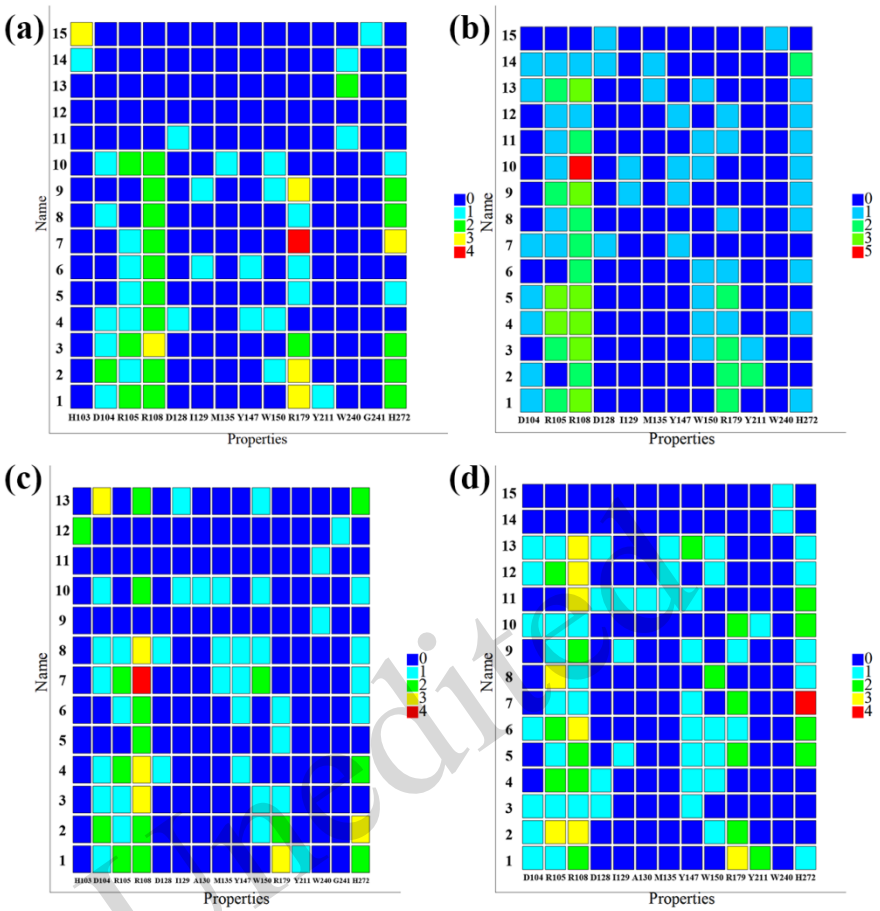

Fig. S5 Docking site heat map

(a)wild type, (b)A142C, (c)S178Q, (d)A181N. From blue to red, the confidence level increases as the numerical value rises.